Check for updates

Designing protein nano-construct in ionic liquid: a boost in efficacy of cytochrome C under stresses†

Sarath Kumar Thayallath,‡[a] Sachin M. Shet,‡[a] Meena Bisht,[b] Pranav Bharadwaj,[a] Matheus M. Pereira, [iD][c] Gregory Franklin, [iD][b] S. K. Nataraj [iD][a] and Dibyendu Mondal [iD] *[ab]

Herein, we present a simple approach to fabricate protein nanoconstructs by complexing cytochrome C (Cyt C) with silk nanofibrils (SNF) and choline dihydrogen phosphate ionic liquid (IL). The peroxidase activity of the IL modified Cyt C nanoconstruct (Cyt C + SNF + IL) increased significantly (2.5 to 10-fold) over unmodified Cyt C and showed enhanced catalytic activity and stability under harsh conditions, proving its potential as a suitable protein packaging strategy.

Enzyme immobilization has been shown to be beneficial in improving the stability of enzymes under harsh reaction conditions.[1] Immobilization of enzymes on nanoscale materials is critical to enhance their catalytic activity.[2] The ability of naturally occurring fibers, especially silk, to alter the surface of various enzymes through bioconjugation has shown great promise.[3] Pranab and his group have shown that silk mats can be used as a biomatrix for the immobilization of cholesterol oxidase.[4] Immobilization of enzymes on electrospun polymer-based nanofibers is also gaining importance nowadays.[5] Biohybrid composites with better activity may have a bright future in biotechnology. However, it has not yet been studied how resistant enzymes are when exposed to various stresses after conjugation with silk fibers. In general, the strong surface modification processes resulted in partial deactivation of the enzymes, which is a major limitation for such a strategy. ILs can also be used as protective media to prevent enzyme unfolding.[6] The addition of osmolytes, especially the use of ionic liquids as co-solvents or solvents, can significantly alter the solvent environment.[7] There are numerous reports of enzyme handling in pure ILs or IL as co-solvents in aqueous solutions.[8,9] Cholinium-based ILs are known to be exceptional solvents for improving the stability of many proteins, which include Cyt C.[10] Compared with other cholinium-based ILs that have been studied for biocatalysis with Cyt C, choline dihydrogen phosphate ([Cho][Dhp]) is considered to be one of the best biocompatible solvents for Cyt C.[11]

The current work highlights the advantages of combining immobilization with silk nanofibrils (SNF) and solvent manipulation with ILs. The major drawback of existing immobilization strategies is irreversible damage due to the strong interaction between the protein and the carrier.[12] ILs are known to induce soft interactions and can therefore be used to reduce this effect.[13] In addition, there are few reports of protein packaging studies involving both protein surface modification and dissolution into ILs.[14] The careful task-specific complexation of Cyt C with SNF and [Cho][Dhp] IL, which have been characterized with various analytical tools, establishes a novel protein surface amendments approach here through the development of protein nanoconstructs. The stability and activity of the protein nanoconstruct (Cyt C + SNF + IL) under extreme temperature conditions, as well as the presence of chemical denaturants (GuHCl) and protease (trypsin), were thoroughly investigated to develop an efficient strategy for protein packaging using a SNF- and IL -based systems. UV-vis, ATR-FTIR, CD and other spectroscopic methods were used to study the stability of the enzyme structure. Molecular docking studies were also performed to investigate how SNF and IL interact with Cyt C. Overall, this study demonstrates the possibility of removing the current limitations on biocatalysis reactions by using SNF and IL as biocompatible media for protein packaging.

To produce SNF from *Bombyx mori* silk fibroin, a pretreatment study was performed. Details of the experimental protocols can be found in the ESI.† Degummed silk fiborin (DGSF), 20 mg mL^{-1} was treated with 46%, 35% and 15% [Cho][OH] IL aqueous solution. It was found that the exfoliation of silk fibroin to SNF was better when 46% of [Cho][OH] was used (Fig. 1a). Microscopic examination (Fig. 1b) confirmed the conversion of silk fibrils to SNFs, as the fibrils were clearly absent or in a much-dissolved

[a] *Centre for Nano and Material Sciences, Jain (Deemed-to-be University), Jain Global Campus, Kanakapura, Bangalore, Karnataka, 562112, India. E-mail: dmtapu@gmail.com, dmon@igr.poznan.pl*

[b] *Institute of Plant Genetics (IPG), Polish Academy of Sciences, Strzeszynska 34, 60-479 Poznan, Poland*

[c] *University of Coimbra, CIEPQPF, Department of Chemical Engineering, Rua Silvio Lima, Polo II – Pinhal de Marrocos, 3030-790 Coimbra, Portugal*
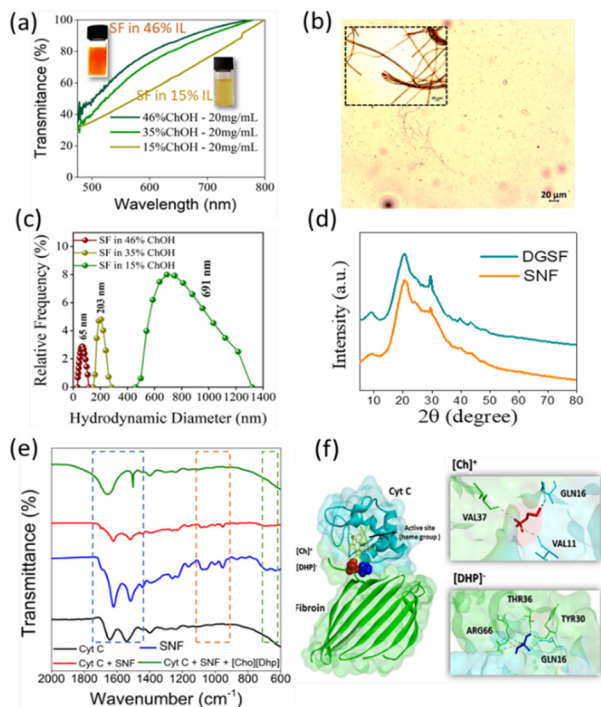
Fig. 1 (a) Silk fibroin exfoliation studies, (b) microscopic images of silk fibrils in presence of [Ch][OH], after 120 min (inset: initial image at 0 min) (the scale bar is 20 micrometer), (c) DLS analysis results for SNF in different concentrations of [Cho][OH], (d) p-XRD analysis results for DGSF and SNF, and (e) ATR-IR results of SNF, IL and SNF + IL and (f) docking pose with the lowermost absolute value of attraction (kcal mol⁻¹) and networking amino acids for Cyt C−fibroin complex with ILs ions.

conditions than on the microscale (inset of Fig. 1b). Dynamic light scattering (DLS) analysis also showed that the fibril diameter was in the nanoscale (65 nm) in the presence of 46% [Ch][OH], which is related to the formation of the SNF composite (Fig. 1c). In addition, the p-XRD spectra of DGSF and SNF were recorded and are shown in Fig. 1d. Both the DGSF and regenerated SNFs showed prominent peaks at $2\theta = 20.4°$ and $29.6°$, respectively (JCPDS no. 89-6096).[15] The peak at $29.6°$ confirms the degumming process and the signal $20.4°$ suggests that the majority of silk fibroin is present in the crystalline β-sheet form. A less intense and broad peak around $24.6°$ indicates the existence of silk-I form comprising of α-helix and β-turns.[16]

Further ATR-FTIR analysis was carried out to understand changes in the functional groups of Cyt C, SNF and [Cho][Dhp] on interaction. Cyt C showed bands ∼1650 cm⁻¹ and ∼1540 cm⁻¹ which are due to amide I stretching mode (C=O) and amide II stretching mode (C–N), respectively.[17] A peak at 1705 cm⁻¹ attributed to the β-turns of the antiparallel β-sheet structure for SNFs at 1630 cm⁻¹ (amide I band) was observed in ATR-IR spectra (Fig. 1e). Further evidence for the presence of the β-sheet after exfoliation and regeneration are the pronounced peaks at 1271 cm⁻¹ (amide III) and 632 cm⁻¹ (amide IV) attributed to the crystalline β-sheet structure.[15] Upon addition of SNF to Cyt C, the intensity of the amide peaks was reduced, suggesting electrostatic interactions between SNF and Cyt C.[18] We can also observe a red shift of the peaks in the range of 1500 to 100 cm⁻¹, which could

be due to a weak hydrogen bonding between SNF and Cyt C.[19] In the case of SNF + IL, an increase in peak intensities was observed, indicating a strong electrostatic interaction between IL and the proteins.[20] Also, the red shift of the peak at 1543 to 1483 cm⁻¹ indicates hydrogen bonding between IL and the proteins.[19] This also confirms the multiple types of interactions between Cyt C, SNF, and IL. To identify protein–protein and protein–protein + ILs ion interactions, a two-step molecular docking analysis was performed. First, the bid alignment of Cyt C and SNF was calculated. The obtained models were assessed and the model with the lesser docking score and ligand rmsd (Å) was chosen. Fig. 1f shows the orientation of the Cyt C−fibroin binding complex. The interacting amino acids of the two proteins, the type of contact, and the geometric distance (Å) are listed in Table S1 (ESI†). H-bond interactions were identified from Cyt C: glutamine and cysteine residues (GLN16 and CYS17) to SNF: threonine and aspartic acid residues (THR36 and ASP29) and from SNF: aspartic acid residues (ASN68 and ASN93) to Cyt C: glutamic acid residues (GLU90). Hydrophobic interactions occur from Cyt C: lysine residue (LYS27) to SNF: phenylalanine residue (PHE26) and from SNF: phenylalanine residues (PHE26 and PHE31) to Cyt C: lysine and cysteine residues (LYS25 and CYS17). Electrostatic interactions were found from Cyt C: lysine residue (LYS87) to SNF: aspartic acid residue (ASP91) and from SNF: arginine residue (ARG66) to Cyt C: phenylalanine residue (PHE82). Finally, the only Pi–sulfur interaction occurs between Cyt C: methionine residue (MET80) and SNF: phenylalanine residue (PHE31). Overall, the Cyt C−SNF complex is driven by a variety of interactions (H-bond, Pi–sulfur, hydrophobic and electrostatic interactions), and the major impact for Cyt C−SNF complex formation come from H-bonding. After identifying the Cyt C−SNF interactions, the effects of the IL ions (cations and anions) and interactions on the Cyt C−SNF complex were evaluated. For this purpose, a molecular docking analysis was performed with a protein–protein complex as receptor and ILs ions as ligands. Fig. 1f shows the binding position with the lowest absolute value of attraction to the Cyt C−SNF structure. The IL (cation and anion individually) docking affinities, interacting amino acid residues, type of contact, and geometric distance (Å) are listed in Table S2 (ESI†). The [Cho]+ shows a higher binding affinity (−3.1 kcal mol⁻¹) compared to the [Dhp]- (−2.7 kcal mol⁻¹). Both IL ions interact with the Cyt C−SNF complex through hydrogen bonds. The [Cho]+ interacts with Cyt C through hydrogen bonds with GLN16 and VAL11 and with SNF at VAL37. In contrast, [Dhp]- interacts with Cyt C−SNF through hydrogen bonds and electrostatic interactions. Hydrogen bonds between [Dhp]- and the protein–protein complex occur with GLN16 of Cyt C, TYR30, THR36, and ARG66 of SNF. In addition, [Dhp]- interacts with the ARG66 residue of SNF through electrostatic interactions.

After the development of the Cyt C nanoconstruct, the effect on its peroxidase activity was investigated using the substrate ABTS (Fig. S1, ESI†). The detailed experimental procedure is provided in the ESI.† In order to operate Cyt C at its maximal velocity (equilibrium), we have used the typical reaction protocol.[6] However, the ILs and the immobilization with SNF might have a great impact on the reaction kinetics of Cyt C.

Fig. S1a, ESI† shows the optimization of [Cho][Dhp] concentration to be employed for manipulating Cyt *C*–SNF complex. 50 µL to 300 µL (2.5% to 15% of IL in distilled water) of [Cho][Dhp] from the stock solution (0.5 g mL^{-1}) was added into the 1 mL of reaction media and it was found that 200 µL (10%) [Cho][Dhp] leads to ∼2.5-fold increase in peroxidase activity compared with native Cyt *C* (Fig. S1a, ESI†). Further, 0.025 to 0.175 mg mL^{-1} SNF solution was added into reaction mixtures to optimize the concentration of SNF. The presence of 0.125 mg mL^{-1} SNF increased the activity of Cyt *C* by 7 times (Fig. S1b, ESI†). Then, by maintaining a constant SNF concentration (0.125 mg mL^{-1}) and altering the quantity of IL, the best combination to get higher activity was optimized (Fig. S1c, ESI†). Optimization studies were also carried out by maintaining a constant IL concentration while changing the SNF concentration (Fig. S1d, ESI†). 0.125 mg mL^{-1} SNF with 50 µL [Cho][Dhp] was optimized as the best combination for increased activity of Cyt *C* in the Cyt *C* + SNF + IL system (Fig. S1c and d, ESI†).

The temperature of the reaction media has a significant impact on the stability and function of enzymes. Accordingly, at temperatures ranging from 30–110 °C, the thermal stability and activity of Cyt *C*, Cyt *C* + SNF, Cyt *C* + IL, and Cyt *C* + SNF + IL were examined. Up to 70 °C, the enzyme activity showed an upward trend, after which it started to decrease. The peroxidase activity of the protein nano-construct was > 7-fold higher than that of native Cyt *C* at a temperature of 110 °C (Fig. 2a), which suggests that manipulation of Cyt *C* with SNF + IL *via* soft interactions can prevent its heat-induced unfolding. In addition, the peroxidase assay was performed at variable pH conditions, which varied from 2–10. The maximum activity was increased ∼7-fold at pH 7 and 8 in the presence of only SNF,

whereas the activity was increased ∼9.5-fold in the presence of both SNF and IL, demonstrating the stabilization of the secondary conformation of Cyt *C*. At acidic pH, the increase in activity was comparatively small due to the degradation of SNF (Fig. 2b).[21] In the presence of 6 M GuHCl, Cyt *C* activity decreases to 15%, whereas it is enhanced in the presence of SNF + IL (Fig. 2c). Addition of 0.125 mg mL^{-1} SNF + 50 µL IL solution increased the relative activity by up to 700%, which is comparatively higher than SNF (600%) and IL (280%). In addition, using the biological denaturant trypsin, the effect on the activity of Cyt *C* was examined in the presence of SNF + IL (Fig. 2d). The activity of Cyt *C* was evaluated 0 hours and 24 hours after incubation with 6 M trypsin at 37 °C. Trypsin was found to reduce Cyt *C* activity by 20%. However, in the presence of SNF + IL, Cyt *C* still had 60% of its original activity. These results suggest that SNF + IL may be helpful in protecting proteins from high temperature and pH, chemical denaturants, and protease-induced biodegradation.

UV-vis spectroscopy analyses were carried out to look into Cyt *C*'s structural stability at high temperatures. Native Cyt *C* has two distinct bands at 280 and 409 nm, which correspond to the n–π⋆ transition of the aromatic amino acids and the π–π⋆ transition of the heme moiety, respectively. Fe is axially linked to the ligands histidine18 and methionine80 in these bands.[11] Peaks at 528 and 550 nm are attributed to the decreased heme protein's π–π⋆ transition (Q bands).[6,11] The decrease in absorbance observed at higher temperatures (90 °C and 110 °C) suggests significant structural changes in the vicinity of the heme group associated with denaturation of the protein. The shift in the Fe-methionine80 residue associated with denaturation of Cyt *C* at higher temperatures caused the Q-band peaks of native Cyt *C* to decrease at higher temperatures (Fig. S2a, ESI†). The presence of the peaks in the Cyt *C* + SNF + IL system indicates that the Cyt *C* structure was preserved even at 110 °C. Similar UV-vis results were obtained when the protein nano-construct was incubated with GuHCl and trypsin (Fig. S2b and c, ESI†). ATR-FTIR spectra were used to further investigate preservation of the secondary structure of Cyt *C*. The protein shows distinct amide I and II bands at 1600–1700 cm^{-1} and 1450–1570 cm^{-1}, respectively. The peak of amide I results from the stretching of the peptide backbones in the C=O direction, whereas the peak of amide II results from the bending of the backbones in the N–H direction.[18,22] At high temperatures, native Cyt *C* lost the distinct amide peaks caused by denaturation of the protein (Fig. S2d, ESI†). However, SNF + IL had no effect on these bands, indicating that the secondary structure of the protein was not disturbed. The results remained the same even with the addition of GuHCl and trypsin (Fig. S2e and f, ESI†). To further understand the potential structural variations of Cyt *C*, CD spectroscopy studies were used to examine the changes in the protein's secondary and tertiary structures in the presence of SNF + IL under various stresses (Fig. 3). The spectra of native Cyt *C* show positive and negative intensity bands at 195–200 nm and 208–222 nm, respectively, both of which indicate significant α-helical secondary structure.[6] The secondary and tertiary structure of Cyt *C* deviates significantly under
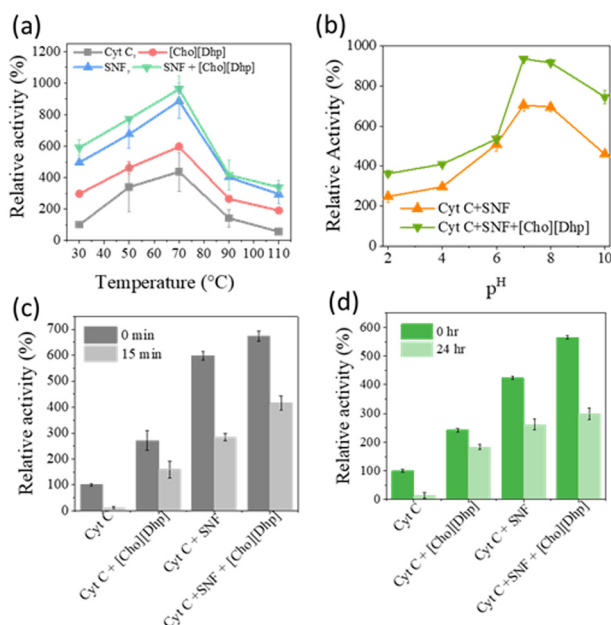

Fig. 2 Peroxidase activity studies of Cyt *C*, Cyt *C* + IL, Cyt *C* + SNF and Cyt *C* + SNF + IL in presence of different stress conditions (a) high temperature (Cyt *C* activity at 30 °C without addition of SNF and IL was considered as 100%), (b) variable pH (Cyt *C* activity at pH 7 without addition of SNF and IL was considered as 100%), (c) GuHCl and (d) Trypsin.
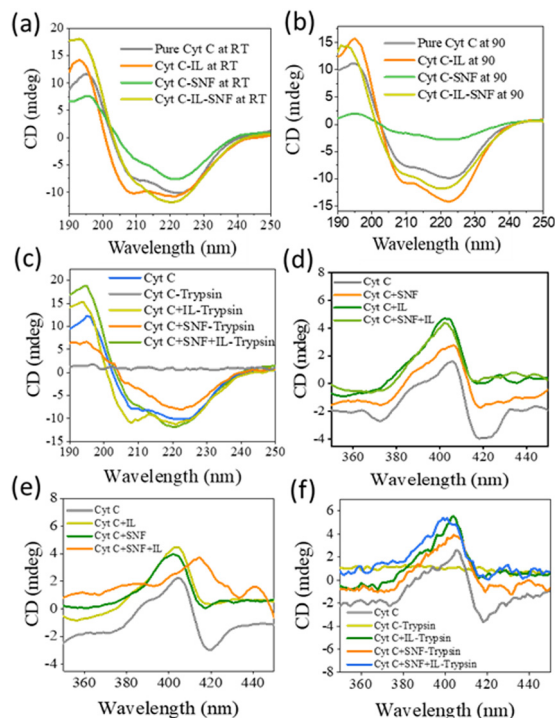
Fig. 3 Far CD spectra of Cyt *C* in presence of (a) room temperature, (b) high temperature and (c) trypsin. Near CD spectra of Cyt *C* in presence of (d) room temperature, (e) high temperature and (f) trypsin.

the different stress conditions, such as extreme temperatures (Fig. 3a and b). In contrast, the secondary structure of Cyt *C* + SNF + IL was stable, as evidenced by the fact that the exclusively negative ellipticity of Cyt *C* did not change, while both the negative and positive bands showed a slight decrease at higher temperatures (Fig. 3b). In the presence of trypsin, Cyt *C* showed denaturation and lost its secondary structure, whereas in the presence of SNF + IL, structural stability was not only maintained but also more stable than Cyt *C* bound only to SNF and IL (Fig. 3c). A look at the Soret band of Cyt *C* (350–450 nm), which provides information about the tertiary structure, confirms the structural integrity of Cyt *C*. After addition of SNF + IL, Cyt *C* maintained its positive and negative bands at 406 and 416 nm, respectively, with no change in the bands around the porphyrin and heme. This indicates that SNF + IL did not significantly alter the conformation of the active site of Cyt *C* (Fig. 3d). In the presence of both SNF and IL and IL, the stability of the tertiary structure was maintained even at high temperatures and in the presence of trypsin, as shown by the results from CD (Fig. 3e and f).

In summary, a facile and novel method for the preparation of protein nanoconstructs combining surface modification by SNF and solvent manipulation by IL was presented. The Cyt *C* + SNF + IL-based system showed an increase in peroxidase activity (2.5 to 10-fold) and improved stability under a variety of processing environments, including extreme heat and the presence of denaturants. Overall, the demonstrated protein nanoengineering protocol is robust for sustainable industrial biocatalysis.

Conflicts of interest

There are no conflicts to declare.

References

1 R. C. Rodrigues, C. Ortiz, Á. Berenguer-Murcia, R. Torres and R. Fernández-Lafuente, *Chem. Soc. Rev.*, 2013, **42**(15), 6290–6307.
2 R. A. Sheldon and S. van Pelt, *Chem. Soc. Rev.*, 2013, **42**(15), 6223–6235.
3 Y. Q. Zhang, *Biotechnol. Adv.*, 1998, **16**(5–6), 961–971.
4 U. Saxena and P. Goswami, *Appl. Biochem. Biotechnol.*, 2010, **162**, 1122–1131.
5 Z. G. Wang, L. S. Wan, Z. M. Liu, X. J. Huang and Z. K. Xu, *J. Mol. Catal. B: Enzym.*, 2009, **56**(4), 189–195.
6 M. Bisht, D. Mondal, M. M. Pereira, M. G. Freire, P. Venkatesu and J. Coutinho, *Green Chem.*, 2017, **19**(20), 4900–4911.
7 O. Russina, F. Lo Celso, N. V. Plechkova and A. Triolo, *J. Phys. Chem. Lett.*, 2017, **8**(6), 1197–1204.
8 A. Brandt, J. Gräsvik, J. P. Hallett and T. Welton, *Green Chem.*, 2013, **15**(3), 550–583.
9 J. N. Pedersen, S. Liu, Y. Zhou, T. Balle, X. Xu and Z. Guo, *Food Chem.*, 2020, **310**, 125858.
10 A. Sindhu, N. K. Mogha and P. Venkatesu, *Int. J. Biol. Macromol.*, 2019, **126**, 1–10.
11 S. M. Shet, S. K. Thayallath, M. Bisht, M. M. Pereira, J. O. A. Coutinho, N. Sanna Kotrappanavar and D. Mondal, *ACS Sustainable Chem. Eng.*, 2021, **9**(24), 8327–8335.
12 D. Remonatto, R. H. M. Júnior, R. Monti, J. C. Bassan and A. V. de Paula, *Process Biochem.*, 2022, **114**, 1–20.
13 S. K. Singh, *Int. J. Biol. Macromol.*, 2019, **132**, 265–277.
14 A. P. Brogan and J. P. Hallett, *J. Am. Chem. Soc.*, 2016, **138**(13), 4494–4501.
15 M. H. Mruthunjayappa, N. S. Kotrappanavar and D. Mondal, *J. Hazard. Mater.*, 2022, **424**, 127561.
16 H.-Y. Wang and Y.-Q. Zhang, *Soft Matter*, 2013, **9**, 138–145.
17 N. Yadav, M. Bisht, S. Nataraj, P. Venkatesu and D. Mondal, *Chem. Commun.*, 2020, **56**(67), 9659–9662.
18 S. M. Shet, P. Bharadwaj, M. Bisht, M. M. Pereira, S. K. Thayallath, V. Lokesh, G. Franklin, N. S. Kotrappanavar and D. Mondal, *Int. J. Biol. Macromol.*, 2022, **215**, 184–191.
19 H. Wang, S. Liu, Y. Zhao, J. Wang and Z. Yu, *ACS Sustainable Chem. Eng.*, 2019, 7(8), 7760–7767.
20 O. S. Hammond and A. V. Mudring, *Chem. Commun.*, 2022, **58**(24), 3865–3892.
21 D. Sargunamani and N. Selvakumar, *Polym. Degrad. Stab.*, 2006, **91**(11), 2644–2653.
22 E. Moe, C. M. Silveira, L. Zuccarello, F. Rollo, M. Stelter, S. De Bonis, C. Kulka-Peschke, S. Katz, P. Hildebrandt and I. Zebger, *Chem. Commun.*, 2022, **58**(90), 12568–12571.